

DYNAMIC FINITE ELEMENT ANALYSIS OF THIRD SIZE CHARPY SPECIMENS OF V-4Cr-4Ti - M. R. Lansberry (University of Missouri-Rolla), R. J. Kurtz (Pacific Northwest National Laboratory), A. S. Kumar (University of Missouri-Rolla), and G. E. Mueller (University of Missouri-Rolla)

OBJECTIVE

The objective of this analysis is to accurately model the behavior of one third size Charpy V-notched (CVN) and fatigue precracked specimens of V-4Cr-4Ti alloys using the dynamic finite element analysis code, ABAQUS / Explicit v5.4 [1].

SUMMARY

A 2-D finite element analysis was performed on precracked, one third scale CVN specimens to investigate the sensitivity of model results to key material parameters such as yield strength, failure strain and work hardening characteristics. Calculations were carried out at temperatures of -196°C and 50°C. The dynamic finite element analyses were conducted using ABAQUS / Explicit v5.4. The finite element results were compared to experimental results [2] for the production-scale heat of V-4Cr-4Ti (ANL Heat #832665) as a benchmark. Agreement between the finite element model and experimental data was very good at -196°C, whereas at 50°C the model predicted a slightly lower absorbed energy than actually measured.

INTRODUCTION

Recent work on A533B pressure vessel steel has indicated that finite element analysis (FEA) can be used to predict the upper shelf energy of precracked, full size CVN specimens using data obtained from subscale specimens to calibrate the model [3]. Furthermore, FEA may also be used to validate empirical correlations for size effects between CVN specimens of various sizes (fracture volume-- $(Bb)^{3/2}$, etc.) [3]. A similar analysis will be performed for V-4Cr-4Ti, a possible fusion power system first wall structural material. A first step in predicting size effects for V-4Cr-Ti is the establishment of a reliable and accurate material model for use in the FEA.

ANALYSIS PROCEDURE

Tensile test data was obtained from the University of California at Santa Barbara [4] on the production-scale heat of V-4Cr-4Ti (ANL Heat #832665). Initially in load-displacement format, data at -196°C and 50°C were converted to true stress-true strain format. A plot of these data is shown in Figure 1. Note the usual yield drop exhibited by bcc metals has been suppressed in this plot.

Since the reduction of area was not measured throughout the tensile test, the curves are only valid up to the ultimate tensile strength of the material. In order to better simulate material behavior during a Charpy impact test, load-displacement data collected at the highest possible strain rate were selected for the FEA. For the 50°C case, the strain rate was 2 s^{-1} while at -196°C, a lower strain rate of 0.02 s^{-1} was used due to high scatter in the 2 s^{-1} strain rate data.

In the ABAQUS / Explicit dynamic fracture mechanics code, material properties play a key role. In Charpy impact studies, for example, the energy absorbed by the material is directly related to the area under the true stress-true strain curve. To achieve an accurate model of such a test, one could simply use point-to-point data as input. Although ABAQUS / Explicit allows this approach, limitations in the material failure criteria require the use of a user defined failure model. In this case, the true stress-

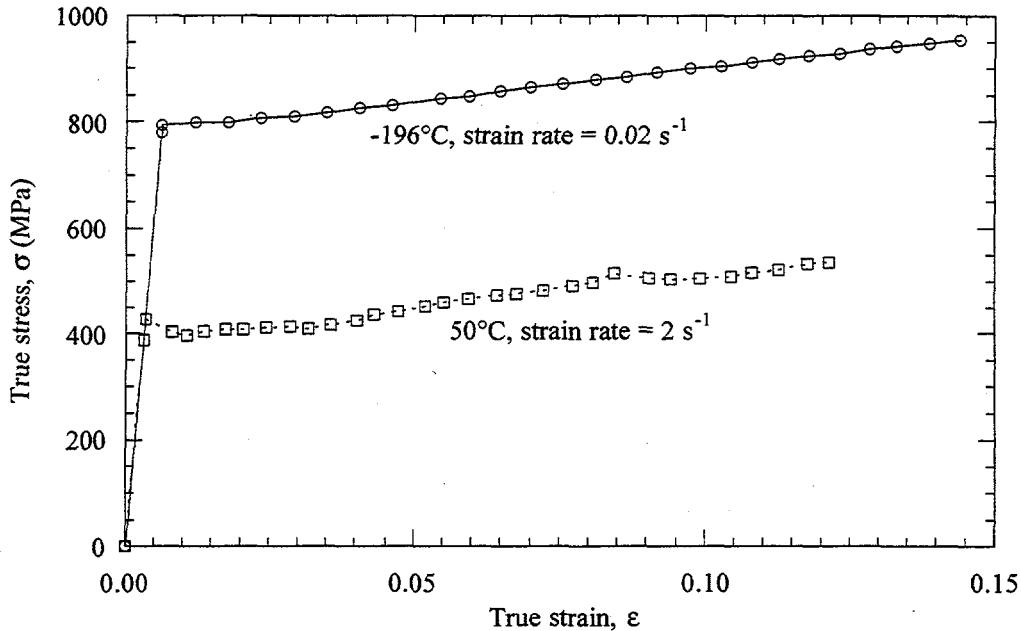


Figure 1 True stress - true strain curves for V-4Cr-4Ti derived from UC Santa Barbara tensile data

true strain data is approximated by a bilinear curve. The general approach is highlighted in Figure 2. As noted in Figure 2, several material properties are required for the bilinear approximation. These include the following Young's modulus, tensile yield strength, Poisson's ratio, hardening modulus (a linear approximation of the work hardening rate), offset failure strain, and the true failure strain.

The Young's modulus and 0.2% yield strength are used to fully describe the elastic region of the true stress-strain curve. In the model, the onset of plastic deformation begins when the elastic limit is exceeded. As plastic deformation of the specimen increases, the metal strain hardens so that the load required to extend the specimen increases with further straining. In order to describe this behavior, the true stress-true strain curve in the plastic region may be approximated by a straight line with a slope denoted as the hardening modulus. This linear behavior continues up to the offset failure strain (ϵ_{ofs}) of the material. The offset failure strain represents the point at which the material **begins** to fail and is slightly less than the true failure strain. The material then unloads gradually to zero until the true failure strain (ϵ_{fs}) is reached. This gradual decline is necessary since an instantaneous drop produces unstable solutions within ABAQUS / Explicit [3]. In general, stable solutions were found to occur when the offset failure strain was approximately 5-10% below the true failure strain. A summary of the material properties used in the FEA for both the -196°C and 50°C cases is given in Table 1.

As noted in Table 1, both the hardening modulus and true failure strain of V-4Cr-4Ti were allowed to vary in a number of cases. Using this approach, the effect of both the hardening modulus and the true failure strain on the Charpy impact absorbed energy could be investigated at different temperatures.

ABAQUS / Explicit was used to analyze a 2-D finite element model of a precracked third size CVN specimen (3.33 mm x 3.33 mm x 25.4 mm). For all cases, the Charpy specimen was precracked to half width (1.665 mm). The finite element model consisted of a very fine mesh with a total of 4,000

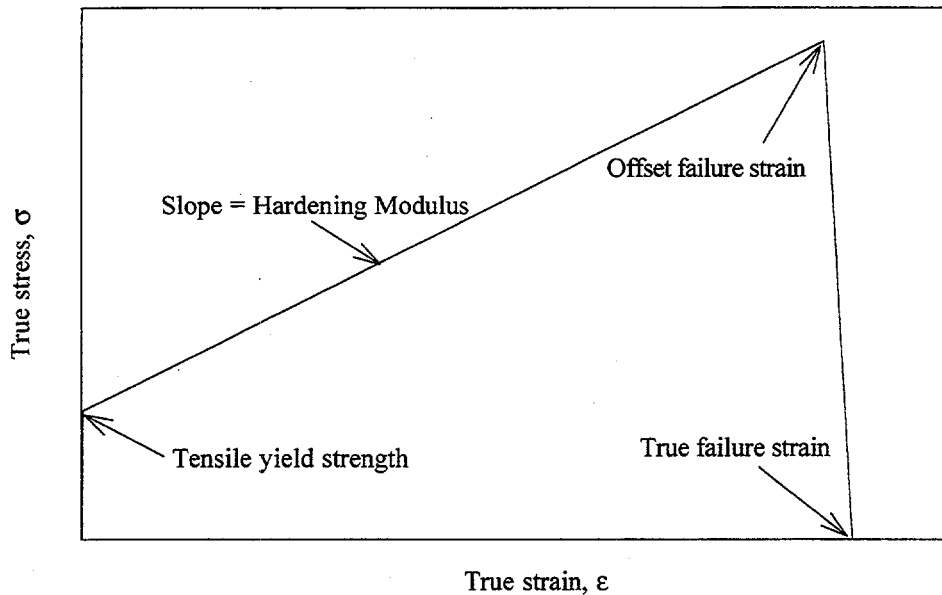


Figure 2 Model true stress - true strain curve for V-4Cr-4Ti

elements making up the Charpy specimen. The striker and anvil were ideally modeled as rigid bodies (i.e., no deformation). As a result, the total energy absorbed by the system was concentrated in the Charpy specimen.

Table 1: V-4Cr-4Ti material properties used in finite element modeling.

Temperature (°C)	Young's Modulus (GPa)	0.2% Yield Strength ⁴ (MPa)	Poisson's Ratio ^{5*}	Hardening Modulus (GPa)	Offset Failure Strain	True Failure Strain
-196	127.3	779.3	0.321	variable	$\epsilon_{fs} - 0.10$	variable
50	124.9	387.4	0.355	variable	$\epsilon_{fs} - 0.10$	variable

* Values were calculated based on the Young's modulus and shear modulus

RESULTS AND DISCUSSION

Argonne National Laboratory (ANL) conducted several Charpy impact tests on both blunt notch and precracked CVN specimens over a wide temperature range [2]. Table 2 summarizes the results of the precracked CVN cases for the production-scale heat of V-4Cr-4Ti. These values were used to benchmark the finite element results.

Normalized energy was calculated based on a fracture volume of $(Bb)^{3/2}$ where B is the thickness of the Charpy specimen and b is the ligament size (= 3.33 mm - Average Crack Length). This method of reporting absorbed energies is recommended per ASTM E23-94b (Standard Test Methods for Notched Bar Impact Testing of Metallic Materials) [6]. Since the finite element model was precracked to half

width in all cases, results from the finite element analyses were normalized to the average crack length values given above to correct for the difference in precrack length. Only the absorbed energies of the finite element model and the ANL experimental data were compared. Finally, results quoted for 50°C stand as is since experimental Charpy data were not available.

Table 2: Summary of combined notch and precracking depths and absorbed energies for ANL production-scale heat #832665 [2].

Impact Temperature (°C)	Crack Length Left (mm)	Crack Length Center (mm)	Crack Length Right (mm)	Crack Length Average (mm)	Absorbed Energy (J)	Normalized Absorbed Energy (J)
-196	1.65	1.66	1.65	1.65	4.34	8.60
-150	1.61	1.63	1.62	1.62	5.59	10.89
-100	1.58	1.60	1.56	1.58	4.86	9.25
21	1.67	1.69	1.70	1.69	3.68	7.47
175	1.64	1.64	1.62	1.64	3.62	7.13

For the first case, the hardening modulus was allowed to vary over a wide spectrum in order to gauge its effect on absorbed energy. During the analysis, the true failure strain was estimated from reduction of area data on the same heat of material [7]. Due to the similar nature of the true stress-true strain curves for the -196°C and 50°C cases, a constant true failure strain of 2.659 was used for both temperatures based on a $\approx 93\%$ reduction of area. The results are shown in Figure 3.

From Figure 3, it is clearly seen that the hardening modulus has only a slight effect on the total absorbed energy even when the hardening modulus values differ by an order of magnitude. There is approximately a 2 J difference between the upper and lower bounds of both curves. In addition, it is a highly linear relationship. Table 3 summarizes the values plotted in Figure 3.

Table 3: Calculated absorbed energy as a function of hardening modulus.

Hardening Modulus (GPa)	Absorbed Energy (J)	
	-196°C	50°C
0.10	2.90	1.79
0.40	3.34	2.18
0.80	3.85	2.61
1.20	4.29	3.03
1.60	4.71	3.43
2.00	5.11	3.83

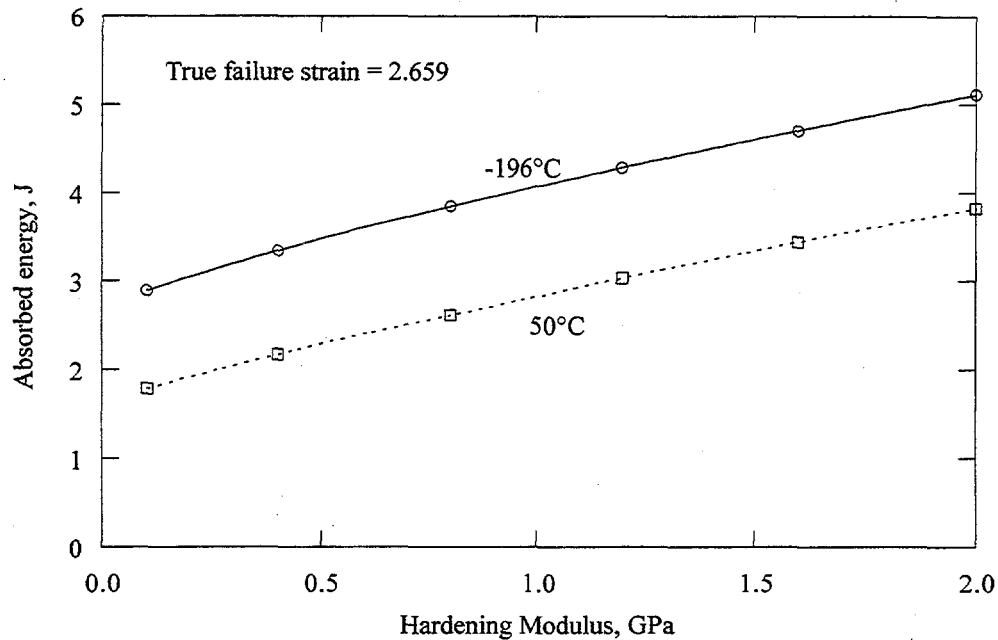


Figure 3 Calculated absorbed energy versus hardening modulus.

The experimentally measured absorbed energies at -196°C and 50°C are 4.34 J and 3.67 J, respectively. The 50°C value was interpolated from the ANL data given in Table 2. From Figure 3, a hardening modulus of about 1.23 GPa at -196°C and 1.80 GPa at 50°C are required for reasonable agreement with the ANL experimental data.

In a similar approach, the true failure strain of the material model was also varied to determine its effect on absorbed energy. For this case, the hardening modulus of the material was calculated from the slope of the plastic strain portion of each true stress-true strain curve. The effect of true failure strain is displayed in Figure 4.

The plot in Figure 4 is very similar in appearance to a DBTT curve. In fact, for a given true failure strain, the model predicts whether ductile or brittle failure will occur. Table 4 summarizes the data points shown in the graph and the fracture behavior predicted by the finite element model.

Table 4: Calculated absorbed energy as a function of true failure strain.

True Failure Strain	Failure Mode*	Absorbed Energy (J)	
		-196°C	50°C
0.30	Complete fracture	0.58	0.45
0.60	Complete fracture	1.58	1.30
1.20	Partial fracture	3.68	2.82
2.40	Pure bending	4.36	3.13

* Both cases exhibited the same failure behavior for the given data points

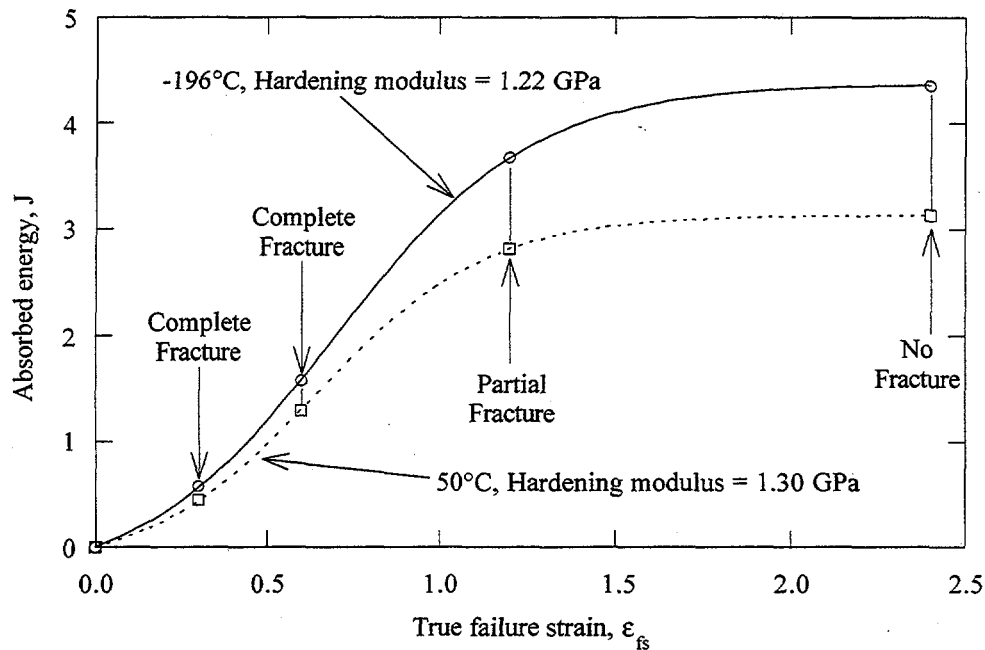


Figure 4 Calculated absorbed energy versus true failure strain.

Agreement between the finite element model and ANL experimental data is very good at -196°C (4.34 J vs. \approx 4.36 J). At 50°C , the finite element model predicts slightly less absorbed energy than the interpolated experimental value (3.67 J vs. \approx 3.12 J). As seen above, the true failure strain plays a significant role in modeling the impact properties of V-4Cr-4Ti.

CONCLUSIONS

- The importance of accurate tensile data in determining a true stress- true strain curve cannot be overstated. It may prove necessary to actually perform a series of tensile tests and specifically measure important quantities such as reduction of area to obtain an accurate measurement of the true failure strain.
- Due to the limited detail present in the bilinear approximation, a better material model could be developed. It may be possible to generate a more accurate approximation of the true stress-true strain curve by defining the curve in a piecewise linear manner.
- Varying the hardening modulus from 0.1 GPa to 2.0 GPa at a true failure strain of 2.659 had a relatively small effect on absorbed energy. Over this range the absorbed energy increased by a factor of 1.8 at -196°C and a factor of 2.1 at 50°C . In contrast, the true failure strain played a more significant role in determining both the absorbed energy and the fracture behavior of the material. Varying the true failure strain from 0.30 to 2.40 changed the absorbed energy by a factor of 7.5 at -196°C and 7.0 at 50°C .

ACKNOWLEDGMENTS

We would like to thank Eric Donahue from the University of California at Santa Barbara for providing

the V-4Cr-4Ti tensile test data.

REFERENCES

1. Hibbit, Karlsson, & Sorensen, Inc., *ABAQUS Explicit Users Manual v5.4*, HKS, 1995.
2. H. M. Chung, L. Nowicki, and D. L. Smith, "Impact Properties of Pre-cracked V-4Cr-4Ti Charpy Specimens," in Fusion Reactor Materials. Semiannual Progress Report, DOE/ER-0313/18, March 31, 1995, Oak Ridge National Laboratory, Oak Ridge, TN, pp. 253-258.
3. S. E. Sidener, *Dynamic Finite Element Analysis of Charpy Impact Tests for use in Nuclear Power Plant Life Extension*, M.S. Thesis, University of Missouri-Rolla, December 1995.
4. R. Odette, E. Donahue and G. Lucas, "Characterization of Fracture Properties of a V-4Cr-4Ti Alloy," presented at the Second IEA Workshop on Vanadium Alloys, Petten, Netherlands, May 20-22, 1996.
5. W. A. Simpson, "Room Temperature Elastic Properties of V-5Cr-5Ti," in Fusion Reactor Materials. Semiannual Progress Report, DOE/ER-0313/16, March 31, 1994, Oak Ridge National Laboratory, Oak Ridge, TN, pp. 258-259.
6. ASTM E23-94b, Standard Test Methods for Notched Bar Impact Testing of Metallic Materials, American Society for Testing and Materials, Philadelphia, PA, 1994, pp. 137-153.
7. H. M. Chung, L. Nowicki, D. Busch, and D. L. Smith, "Tensile Properties of V-(4-5)Cr-(4-5)-Ti Alloys," in Fusion Reactor Materials. Semiannual Progress Report, DOE/ER-0313/19, December 31, 1995, Oak Ridge National Laboratory, Oak Ridge, TN, pp. 17-21.